

# Spectrum concentration in deep residual learning: a free probability approach

Zenan Ling<sup>1</sup>, Xing He<sup>1</sup>, Robert C. Qiu<sup>1,2</sup>, *Fellow, IEEE*

## Abstract

We revisit the weight initialization of deep residual networks (ResNets) by introducing a novel analytical tool in free probability to the community of deep learning. This tool deals with the limiting spectral distribution of *non-Hermitian* random matrices, rather than their conventional *Hermitian* counterparts in the literature. This new tool enables us to evaluate the singular value spectrum of the input-output Jacobian of a fully-connected deep ResNet in both linear and nonlinear cases. With the powerful tool of free probability, we conduct an asymptotic analysis of the (limiting) spectrum on the single-layer case, and then extend this analysis to the multi-layer case of an arbitrary number of layers. The asymptotic analysis illustrates the necessity and universality of rescaling the classical random initialization by the number of residual units  $L$ , so that the squared singular value of the associated Jacobian remains of order  $O(1)$ , when compared with the large width and depth of the network. We empirically demonstrate that the proposed initialization scheme learns at a speed of orders of magnitudes faster than the classical ones, and thus attests a strong practical relevance of this investigation.

## Index Terms

Residual network, weight initialization, random matrix theory, non-Hermitian free probability theory, Jacobian matrix, spectral density.

## I. INTRODUCTION

Deep neural networks have obtained impressive achievements in numerous fields from computer vision [1] to speech recognition [2] and natural language processing [3]. Yet for all the successes won with these deep structures, we have gained only a rudimentary theoretical understanding of why and in what contexts they work well. Modern deep neural networks are typically trained with gradient-based methods, where the (weight) initialization plays a crucial role in the efficient training of those deep models, as a result of the highly non-convex nature of the underlying objective function. Prior works [4]–[6] have shown that, to prevent gradients from vanishing or exploding (which is believed to be the main difficulty in training deeper models that have more expressive power than shallower ones), one shall choose a proper initialization so that the deep network’s input-out Jacobian is well-conditioned. In other words, in order to preserve the norm of a randomly chosen error vector through backpropagation, the squared singular values of the Jacobian matrix shall remain to be the order of  $O(1)$ , compared with the (possibly) tremendous width or depth of the network. We refer to this property as the “Spectrum Concentration” of the Jacobian matrix, that is different from the similar concept of “Dynamical Isometry” [7] demanding that *all* singular values remain close to 1.

In particular, ResNet, as one of the most popular modern deep network structures, has achieved the state-of-the-art performance on various challenging tasks [8], [9]. Nonetheless, it is worthy noting that in practice the He initialization [5] and the batch normalization (BN) technique [10] are commonly combined together to ensure an effective training of ResNets. Experiments in Fig. 1 show, on the other hand, that the input-output Jacobian of a fully-connected ResNet (without BN) with He’s initialization can be ill-conditioned, in the sense that most singular values are close to zero, while many extremely large singular values lie in a heavy tail away from zero. This occurs even at the *beginning* of the training procedure. Recall that, before the introduction of BN, various of deep networks have been successfully designed and trained without this catastrophic problem of exploding or vanishing gradients. This surprising empirical result naturally leads to the following question:

*Have we really used the “good” initialization for ResNets?*

Among the commonly used random initialization schemes, the variances  $\sigma_w^2$  of the Gaussian weights are *always* normalized by the numbers of neurons of the corresponding layer (i.e., the *width*  $N$  of the network, for example in the case of He’s initialization  $\sigma_w^2 = \frac{2}{N}$ ). In contrast, the number of layers of the network (i.e., its *depth*  $L$ ), as another crucial parameter, has been rarely taken into account. In this article, exploiting advanced tools in random matrix theory in the regime of large network width and depth, we prove that, for ResNets, the variance of the random weights should also be scaled as a function of the number of layers, so as to prevent the gradients vanishing or exploding problem via spectrum concentration.

This work was partly supported by NSF of China No. 61571296 and (US) NSF Grant No. CNS-1619250.

<sup>1</sup> Department of Electrical Engineering, Center for Big Data and Artificial Intelligence, State Energy Smart Grid Research and Development Center, Shanghai Jiaotong University, Shanghai 200240, China. (e-mail: lingzenan@sjtu.edu.cn; rcqiu@sjtu.edu.cn).

<sup>2</sup> Department of Electrical and Computer Engineering, Tennessee Technological University, Cookeville, TN 38505, USA. (e-mail:rcqiu@tntech.edu).

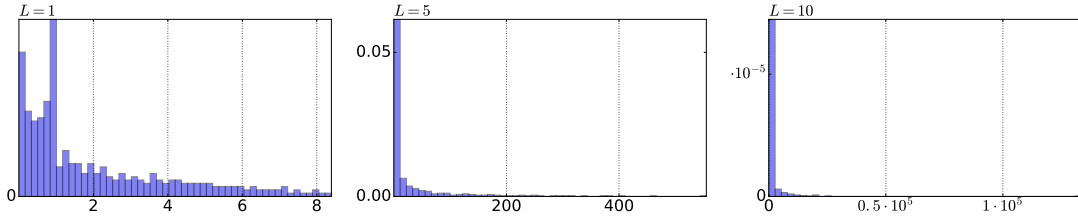


Fig. 1: Empirical eigenvalue density of  $\mathbf{J}\mathbf{J}^T$  with  $\mathbf{J}$  the input-output Jacobian of a fully connected (untrained) ResNet of width  $N = 400$  and depth  $L = 1, 5, 10$  with  $\sigma_w^2 = 2$ .

### A. Related work

The authors in [7] start the consideration of the ill-conditioned Jacobian from random Gaussian initialization, and propose to use orthogonal weights initialization to achieve dynamical isometry in deep *linear* networks. The recent works [6], [11] open the door for a direct application of random matrix theory, particularly *free probability*, to evaluating the Jacobian spectrum of a deep network, in which the singular value distribution of the Jacobian of a fully-connected network is analytically given as a function of depth, random initialization and nonlinearity. In [12] the authors prove the existence of a global optimal solution for linear ResNet, if the spectral norms of the weights are bounded by  $O(1/L)$  and therefore, small random weights that is normalized by the layer number  $L$ , helps deep residual learning. In [13], the authors investigate the forward and backward signal propagation of ResNet using mean field theory and discuss the importance of the  $O(1/L)$  scaling. However, the mean-field analysis only predicts the expectation of the Jacobian spectrum while the higher moments and the full distribution are not considered by the authors. In [14], the authors discuss the universal characters of the singular spectrum under the  $O(1/L)$  scaling with free probability. This work is related to ours but the derivation become tractable only by pre-assuming  $\sigma_w^2 = O(1/L)$  and the necessity of the  $O(1/L)$  scaling, and more general initialization settings, are not discussed in their work. Some similar results are presented in III-C for completeness.

### B. Our contributions

Based on recent advances in free probability theory, we establish a general framework for the spectral analysis of the input-output Jacobian of a ResNet, for Gaussian and orthogonal random initialization with various nonlinear activation functions. The conditions for *necessity* and *universality* of taking  $\sigma_w^2 = O(1/L)$  is unified under the proposed analysis framework.

More concretely, we extend the framework established in [6] to a non-Hermitian setting so as to overcome the (non-trivial) technical difficulty (mentioned in III-A) arising from studying the spectrum of the input-output Jacobian of a single layer ResNet. This result is then extended to the multi-layer case, for which we calculate the expectation and variance of the *full* spectrum. The results of the expectation and variance demonstrates the necessity of taking  $\sigma_w^2 = O(1/L)$  to ensure the aforementioned key property of spectrum concentration to facilitate training. Furthermore, the full spectrum characterization in the case of  $\sigma_w^2 = O(1/L)$  is provided. The result illustrates that it suffices to take  $\sigma_w^2 = O(1/L)$  to ensure the squared singular values of the aforementioned Jacobian to be of order  $O(1)$ , for both random Gaussian and orthogonal weights with *any* nonlinearity, which meets some mild assumption. The theoretical results are corroborated by empirical evidences on popular CIFAR-10 dataset [15]. For the sake of simplicity, some detailed proofs and complementary experiments are deferred to Appendix.

## II. PROBLEM STATEMENT AND PRELIMINARIES

### A. Problem set up

Denote the output vector of the  $(l-1)$ -th layer  $\mathbf{x}^{l-1} \in \mathbb{R}^N$ , weight matrix  $\mathbf{W}^l \in \mathbb{R}^{N \times N}$ , bias vector  $\mathbf{b}^l \in \mathbb{R}^N$  of the layer  $l$  and pre-activation  $\mathbf{h}^l$ , then the forward dynamics of a fully connected ResNet without BN of depth  $L$  is given by:

$$\begin{aligned} \mathbf{h}^l &= \mathbf{W}^l \mathbf{x}^{l-1} + \mathbf{b}^l, \\ \mathbf{x}^l &= \mathbf{x}^{l-1} + \phi(\mathbf{h}^l), \quad \text{for } l = 1, \dots, L, \end{aligned} \quad (1)$$

where  $\mathbf{x}_0 \in \mathbb{R}^N$  is the input data of the network and  $\phi: \mathbb{R} \mapsto \mathbb{R}$  denotes the pointwise nonlinearity. The associated input-output Jacobian is given by

$$\mathbf{J} = \frac{\partial \mathbf{x}^L}{\partial \mathbf{x}^0} = \prod_{l=1}^L (\mathbf{I}_N + \mathbf{D}^l \mathbf{W}^l). \quad (2)$$

with diagonal  $\mathbf{D}^l$  such that  $\mathbf{D}_{ii}^l = \phi'(\mathbf{x}_i^{l-1})$ .

We are interested in the initial state of the training procedure of a ResNet described in (1) by considering two popular random weight initializations: random Gaussian weights with  $\mathbf{W}_{ij}^l \sim \mathcal{N}(0, \sigma_w^2/N)$ , and random orthogonal weights that satisfies  $\mathbf{W}^l (\mathbf{W}^l)^T = \sigma_w^2 \mathbf{I}_N$ .

For nonlinearity, we make two wild assumptions that  $\int \phi'(x)^2 \mathcal{D}x \neq 0$  and  $\int \phi(x) \mathcal{D}x$  is non-negative, where  $\mathcal{D}x = e^{-\frac{x^2}{2}} dx / \sqrt{2\pi}$  denotes the standard Gaussian measure. Note that almost all of the frequently-used activation functions meet these conditions.

Moreover, following several related work [6], [13], [16], we make a *key assumption* that the weights in the forward and backward propagation are independent. Mathematically, this assumption is incorrect because the activations of deeper layers depend explicitly on the weight matrices of shallower layers. However, theoretical computations become tractable under this assumption and the empirical results show a strong support for it. There must be a phase transition that this assumption breaks down after some training steps. Quantitatively controlling this approximation may be quite complicated and we leave this investigation to the future work.

### B. Signal propagation

For large  $N$ , the empirical distribution of  $\mathbf{h}_i^l$  converges to a zero mean Gaussian since that each  $\mathbf{h}^l = \mathbf{W}^l \mathbf{x}^{l-1} + \mathbf{b}^l$  is a weighted sum of a large number of uncorrelated random variable, i.e., the weights and biases which are independent of the activation in previous layers. Let  $q^l \equiv \frac{1}{N} \sum_{i=1}^N (\mathbf{h}_i^l)^2$  denotes the variance of the pre-activation  $\mathbf{h}^l$ . For ResNet (1), the recursive equation for  $q^l$  is given by,

$$\begin{aligned} q^{l+1} = & q^l + \sigma_w^2 \int \phi^2(\sqrt{q^l} x) \mathcal{D}x \\ & + 2\sigma_w^2 \left[ \sum_{k=0}^{l-1} \int \phi(\sqrt{q^k} x) \mathcal{D}x \right] \int \phi(\sqrt{q^l} x) \mathcal{D}x, \end{aligned} \quad (3)$$

with initial condition  $q^0 = \frac{1}{N} \sum_{i=1}^N (\mathbf{h}_i^0)^2$ .

The detailed derivation for the equivalent argument is provided in [13], [14]. The recursion relation (3) for ResNets is essentially different from that of a fully-connected vanilla neural network without residual connection that the biases have no influence. Moreover, one can easily observe that  $q^{l+1}$  is a result of adding positive terms to the previous  $q^l$ . Thus, the variance of pre-activations grows with the depth and *no non-trivial fixed point exists* in the recursion (3).

### C. Hermitian free probability theory

Free probability generalizes probability theory to algebras of non-commutative random variables, which is notably the case of the algebra of random matrices [17], [18]. When a pair of random matrices is free, the eigenvalue distribution of their combinations (sum, product, etc.) can then be determined through specific analytical tools, introduced next.<sup>1</sup>

The spectral density of a random Hermitian matrix  $\mathbf{X} \in \mathbb{R}^{N \times N}$  is defined as  $\rho_{\mathbf{X}}(\lambda) = \frac{1}{N} \sum_{k=1}^N \delta(\lambda - \lambda_k(\mathbf{X}))$ , where  $\lambda_k(\mathbf{X})$  ( $k = 1, \dots, N$ ) denote the  $N$  eigenvalues of  $\mathbf{X}$ . The limiting spectral density is defined as the limit of  $\rho_{\mathbf{X}}(\lambda)$  as  $N \rightarrow \infty$ , if it exists.

The Stieltjes transform of  $\rho_{\mathbf{X}}$  is defined as

$$G_{\mathbf{X}}(z) \equiv \int_{\mathbb{R}} \frac{\rho_{\mathbf{X}}(t)}{z-t} dt, \quad (4)$$

where  $z \in \{z : z \in \mathbb{C}, \Im(z) > 0\}$ . The spectral density can be recovered from the Stieltjes transform using the inversion formula,

$$\rho_{\mathbf{X}}(\lambda) = -\frac{1}{\pi} \lim_{\epsilon \rightarrow 0^+} \Im G_{\mathbf{X}}(\lambda + i\epsilon). \quad (5)$$

The Stieltjes transform can be typically expanded into a power series as

$$G_{\mathbf{X}}(z) = \sum_{k=0}^{\infty} \frac{m_k}{z^k}, \quad (6)$$

with the matrix moments

$$m_k = \int \rho(\lambda) \lambda^k d\lambda, \quad (7)$$

which further determine the moment generating function  $M_{\mathbf{X}}$  (also referred to as the M-transform) of the random matrix  $\mathbf{X}$ ,

$$M_{\mathbf{X}}(z) = zG_{\mathbf{X}}(z) - 1 = \sum_{k=1}^{\infty} \frac{m_k}{z^k}. \quad (8)$$

And the S-transform of  $\mathbf{X}$  is defined as,

$$S_{\mathbf{X}}(z) \equiv \frac{1+z}{zM_{\mathbf{X}}^{-1}(z)}. \quad (9)$$

<sup>1</sup> In the section that follows, the argument  $z$  will be frequently dropped for notational simplicity.  $f^{-1}$  denotes the functional inverse of  $f$ .

The power series  $G_{\mathbf{X}}(z)$  can be inverted (for composition of formal power series), in the form,

$$G_{\mathbf{X}}^{-1}(z) = \frac{1}{z} + \frac{1}{z} \sum_{k=1}^{\infty} r_k z^k = \frac{1}{z} + R_{\mathbf{X}}(z). \quad (10)$$

The power series  $R_{\mathbf{X}}(z)$  is called the R-transform of  $\mathbf{X}$  and its coefficients are called the free cumulants. For any two freely independent non-commutative random variables  $\mathbf{X}, \mathbf{Y}$ , the R- and S-transform have the following definite (convolution) properties,

$$R_{\mathbf{X}+\mathbf{Y}}(z) = R_{\mathbf{X}}(z) + R_{\mathbf{Y}}(z), \quad (11)$$

$$S_{\mathbf{X}\mathbf{Y}}(z) = S_{\mathbf{X}}(z)S_{\mathbf{Y}}(z). \quad (12)$$

As such, the R-transform *linearizes* free additive convolution and the S-transform of the matrix multiplication  $\mathbf{X}\mathbf{Y}$  is simply the multiplication of their S-transforms.

Moreover, R- and S-transforms relate through [17],

$$S_{\mathbf{X}}(zR_{\mathbf{X}}(z)) = \frac{1}{R_{\mathbf{X}}(z)}. \quad (13)$$

#### D. Non-Hermitian free probability theory

Consider the single layer case in our problem. Let  $\mathbf{J}_l := \mathbf{I} + \mathbf{D}^l \mathbf{W}^l$  denotes the input-output Jacobian matrix of the layer  $l$ . Expand  $\mathbf{J}_l \mathbf{J}_l^T$  and we have that

$$\mathbf{J}_l \mathbf{J}_l^T = \mathbf{I} + \mathbf{D}^l \mathbf{W}^l (\mathbf{W}^l)^T \mathbf{D}^l + \mathbf{D}^l \mathbf{W}^l + (\mathbf{W}^l)^T \mathbf{D}^l. \quad (14)$$

Note that the objective of interest  $\mathbf{J}_l \mathbf{J}_l^T$  is *Hermitian* but the resulting four terms of expansion are *not freely independent* and thus can not be handled with a single R-transform. On the other hand, the term in  $\mathbf{J}_l$  are *free* but they are *non-Hermitian*. As such, we perform an extension of conventional (Hermitian) free probability to non-Hermitian random matrices [19] to evaluate the limiting eigenvalue distribution of  $\mathbf{J}_l \mathbf{J}_l^T$ .

Consider a Hermitian matrix  $\tilde{\mathbf{X}}$  such that the eigenvalue distribution of  $\tilde{\mathbf{X}}$  is

$$\rho_{\tilde{\mathbf{X}}}(\lambda) = \frac{\rho_{\sqrt{\mathbf{X}\mathbf{X}^T}}(\lambda) + \rho_{\sqrt{\mathbf{X}\mathbf{X}^T}}(-\lambda)}{2} \quad (15)$$

where  $\tilde{\mathbf{X}}$  is symmetrized singular value version of  $\mathbf{X}$ . The following equation establishes the connection between  $\tilde{\mathbf{X}}$  and  $\mathbf{X}\mathbf{X}^T$ ,

$$G_{\tilde{\mathbf{X}}}(z) = zG_{\mathbf{X}\mathbf{X}^T}(z^2), \quad (16)$$

A random matrix  $\mathbf{X}$  is called *R-diagonal* if it can be decomposed as  $\mathbf{X} = \mathbf{U}\mathbf{Y}$ , such that  $\mathbf{U}$  is Haar unitary and free of  $\mathbf{Y} = \sqrt{\mathbf{X}\mathbf{X}^T}$ . If the free random matrices  $\mathbf{X}$  and  $\mathbf{Y}$  are R-diagonal, then we have,

$$R_{\widetilde{\mathbf{X}+\mathbf{Y}}} = R_{\tilde{\mathbf{X}}} + R_{\tilde{\mathbf{Y}}}. \quad (17)$$

where  $R_{\tilde{\mathbf{X}}}(z) = \sum_{k=1}^{\infty} r_{2k-1} z^k$  generates the cumulants  $r_{2k-1}$ .

For a random matrix  $\mathbf{X}$ , the S-transforms of  $\tilde{\mathbf{X}}$  and  $\mathbf{X}\mathbf{X}^T$  have the following relation:

$$S_{\tilde{\mathbf{X}}}(z) = \sqrt{\frac{z+1}{z}} S_{\mathbf{X}\mathbf{X}^T}(z). \quad (18)$$

### III. THEORETICAL RESULTS

Equipped with the aforementioned free probability tool, we are in the position to study the asymptotic spectrum of the Jacobian matrix in the simultaneously large  $N, L$  limit. As mentioned in Section II-B, *no non-trivial fixed point exists* in the recursion (3) and we can not simply assume that  $\mathbf{D}^l$  equals to each other as in the case of vanilla fully connected networks [6], [11]. Thus, we provide the analysis for the single layer first and extend the result to the multi layer case through S-transform and power series expansion. The necessity of taking  $\sigma_w^2 = O(1/L)$  is proved by investigating the expectation and variance of the spectral density distribution. Finally, the universality of taking  $\sigma_w^2 = O(1/L)$  is discussed by investigating the full spectrum characterization.

### A. Single layer case

First, we deduce the equation for solving the Stieltjes transform  $G_{\mathbf{J}_l \mathbf{J}_l^\top}$  of  $\mathbf{J}_l \mathbf{J}_l^\top$ . According to [19], we have

$$G_{\mathbf{J}_l \mathbf{J}_l^\top} = G_{(\mathbf{I} + \mathbf{D}^l \mathbf{W}^l)(\mathbf{I} + \mathbf{D}^l \mathbf{W}^l)^\top} = G_{(\mathbf{U} + \mathbf{D}^l \mathbf{W}^l)(\mathbf{U} + \mathbf{D}^l \mathbf{W}^l)^\top}, \quad (19)$$

where  $\mathbf{U}$  is a random Haar unitary matrix and free of  $\mathbf{W}^l \mathbf{D}^l$ . Note that  $\widetilde{\mathbf{U}}$  and  $\widetilde{\mathbf{D}^l \mathbf{W}^l}$  are R-diagonal, with (17) we have,

$$R_{\mathbf{U} + \widetilde{\mathbf{D}^l \mathbf{W}^l}}(z) = R_{\widetilde{\mathbf{U}}}(z) + R_{\widetilde{\mathbf{D}^l \mathbf{W}^l}}(z). \quad (20)$$

According to the definition of R-transform (10), we have,

$$z = R_{\widetilde{\mathbf{U}}} \left[ G_{\mathbf{U} + \widetilde{\mathbf{D}^l \mathbf{W}^l}}(z) \right] + R_{\widetilde{\mathbf{D}^l \mathbf{W}^l}} \left[ G_{\mathbf{U} + \widetilde{\mathbf{D}^l \mathbf{W}^l}}(z) \right] + \frac{1}{G_{\mathbf{U} + \widetilde{\mathbf{D}^l \mathbf{W}^l}}(z)} \quad (21)$$

With (16), we have,

$$G_{\mathbf{J}_l \mathbf{J}_l^\top} = G_{(\mathbf{U} + \mathbf{D}^l \mathbf{W}^l)(\mathbf{U} + \mathbf{D}^l \mathbf{W}^l)^\top}(z) = \frac{1}{\sqrt{z}} G_{\mathbf{U} + \widetilde{\mathbf{D}^l \mathbf{W}^l}}(\sqrt{z}). \quad (22)$$

By substitute (22) to (21), we have the following theorem.

**Theorem 1** (Single layer case). For all  $z \in \mathbb{C}$  with positive imaginary part, denote  $G_{\mathbf{J}_l \mathbf{J}_l^\top}(z)$  the (limiting) Stieltjes transform of  $\mathbf{J}_l \mathbf{J}_l^\top$ . Then, as  $N \rightarrow \infty$ , we have

$$\begin{aligned} & \sqrt{z} G_{\mathbf{J}_l \mathbf{J}_l^\top}(z) \left[ R_{\widetilde{\mathbf{U}}} \left( \sqrt{z} G_{\mathbf{J}_l \mathbf{J}_l^\top}(z) \right) + R_{\widetilde{\mathbf{D}^l \mathbf{W}^l}} \left( \sqrt{z} G_{\mathbf{J}_l \mathbf{J}_l^\top}(z) \right) \right] \\ & = z G_{\mathbf{J}_l \mathbf{J}_l^\top}(z) - 1, \end{aligned} \quad (23)$$

where  $\mathbf{U}$  is a random Haar unitary matrix and free of  $\mathbf{D}^l \mathbf{W}^l$ . The correct root is selected by the asymptotic behavior  $G_{\mathbf{J}_l \mathbf{J}_l^\top}(z) \sim \frac{1}{z}$  as  $z \rightarrow \infty$  [18].

Based on Theorem. 1, the detailed procedure for calculating the density of  $\mathbf{J}_l \mathbf{J}_l^\top$  is summarized as follows:

- 1) Calculate  $M_{\mathbf{D}^l}(z)$  with (8), then calculate  $S_{\mathbf{D}^l}(z)$  with (9);
- 2) Calculate  $S_{\mathbf{D}^l \mathbf{W}^l(\mathbf{D}^l \mathbf{W}^l)^\top}(z)$  with (12);
- 3) Calculate  $S_{\widetilde{\mathbf{U}}}(z)$  and  $S_{\widetilde{\mathbf{D}^l \mathbf{W}^l}}(z)$  with (18);
- 4) Calculate  $R_{\widetilde{\mathbf{U}}}(z)$  and  $R_{\widetilde{\mathbf{D}^l \mathbf{W}^l}}(z)$  with (13);
- 5) Calculate  $G_{\mathbf{J}_l \mathbf{J}_l^\top}(z)$  with (23);
- 6) Calculate the spectral density with (5).

The calculation of  $S_{\mathbf{D}^l \mathbf{W}^l(\mathbf{D}^l \mathbf{W}^l)^\top}(z)$  in step 2 requires the information of  $S_{\mathbf{W}^l(\mathbf{W}^l)^\top}(z)$  and  $M_{\mathbf{D}^l}^2(z)$ . For scaled Gaussian weights, the spectral density distribution follows the famous *Marchenko-Pastur Law* (M-P Law) [20],

$$\rho_{\mathbf{W}^l(\mathbf{W}^l)^\top}(\lambda) = \frac{\sqrt{(4\sigma_w^2 - \lambda)\lambda}}{2\pi\sigma_w^2}, \quad (24)$$

for  $\lambda \in [0, 4\sigma_w^2]$ . Through (4), (8) and (12), it is easy to deduce that,

$$S_{\mathbf{W}^l(\mathbf{W}^l)^\top}(z) = \frac{1}{\sigma_w^2(1+z)}. \quad (25)$$

For scaled orthogonal weights, it is obvious that

$$\rho_{\mathbf{W}^l(\mathbf{W}^l)^\top}(\lambda) = \delta(\lambda - \sigma_w^2). \quad (26)$$

Using (4), (8) and (12) again, we obtain  $S_{\mathbf{W}^l(\mathbf{W}^l)^\top}(z) = 1$ .

Moreover,  $\mathbf{D}^l$  is a diagonal matrix with  $\mathbf{D}_{ii}^l = \phi'(\mathbf{h}_i^{l-1})$ , so  $\phi'(\mathbf{h}_i^{l-1})^2$  is the eigenvalue of  $(\mathbf{D}^l)^2$ . The empirical distribution of pre-activations  $\mathbf{h}_i^l$  converges to a Gaussian with zero mean and variance  $q^l$ , in the large N limit. Therefore, for any nonlinearity  $\phi(x)$ , we have, through (4) and (8),

$$M_{\mathbf{D}^l}^2(z) = \int \frac{\phi'(\sqrt{q^l}x)^2}{z - \phi'(\sqrt{q^l}x)^2} \mathcal{D}x. \quad (27)$$

In Fig. 2, we plot the empirical eigenvalue density of  $\mathbf{J}_l \mathbf{J}_l^\top$  (in purple) and the limiting distribution (in red) calculated from the above procedure, for Gaussian and orthogonal weights with  $\sigma_w^2 = 0.1$  or 1,  $\phi(x) = \text{ReLU}(x)$  or  $x$ .

In principle, this procedure can be carried out for an arbitrary choice of nonlinearity so that we can deduce the limiting spectral distribution for  $\mathbf{J}_l \mathbf{J}_l^\top$  for any  $\phi(\cdot)$ . However, the solution of (23) can be really complicated and unenlightening, and

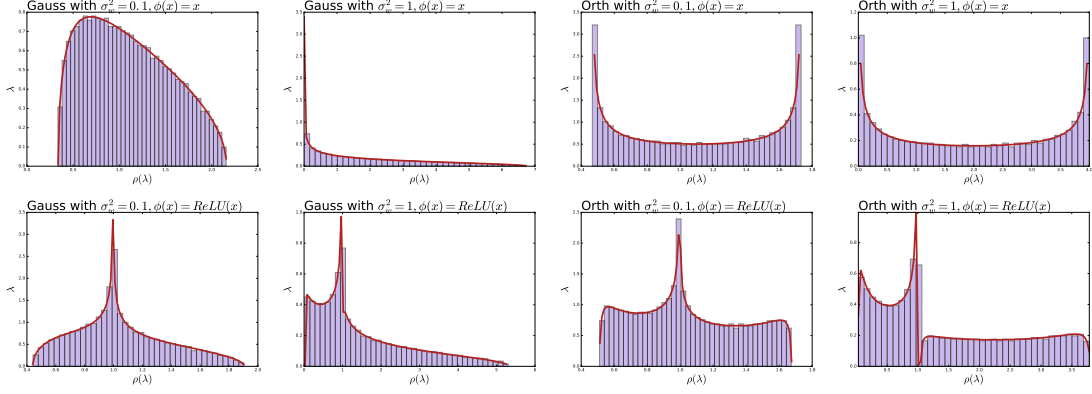


Fig. 2: Empirical eigenvalue density (purple) and limiting distribution (red) procedure of  $\mathbf{J}_l \mathbf{J}_l^T$  for Gaussian and orthogonal weights with  $N = 400$ ,  $\sigma_w^2 = 0.1$  and  $1$ .

thus the calculation for multi-layer case can not be carried out. Inspired by [11], we investigate the lower moments, i.e., the expectation  $\mu_{\mathbf{J}_l \mathbf{J}_l^T}$  and variance  $\sigma_{\mathbf{J}_l \mathbf{J}_l^T}^2$ , of the limiting eigenvalue density of  $\mathbf{J}_l \mathbf{J}_l^T$  instead.

Note that the cumulants of  $R_{\widetilde{\mathbf{D}^l \mathbf{W}^l}}(z)$  can be calculated in terms of the series expansions of  $S_{\mathbf{W}^l (\mathbf{W}^l)^T}(z)$  and  $M_{\mathbf{D}^{l2}}(z)$ , which are defined as,

$$S_{\mathbf{W}^l (\mathbf{W}^l)^T}(z) \equiv \sigma_w^{-2} \left( 1 + \sum_{k=1}^{\infty} s_k z^k \right), \quad (28)$$

$$M_{\mathbf{D}^{l2}}(z) \equiv \sum_{k=1}^{\infty} d_k^{(l)} z^{-k}, \quad (29)$$

where the moments of  $\mathbf{D}^{l2}$  are given by

$$d_k^{(l)} = \int \left[ \phi'(\sqrt{q^l} x) \right]^{2k} \mathcal{D}x. \quad (30)$$

Moreover, both the Stieltjes and R-transform in (23) can be expanded into power series. Thus, we can obtain the low order moments by expanding (23). After a tedious manipulation, we get the first and second order moment of the spectral density of  $\mathbf{J}_l \mathbf{J}_l^T$ ,

$$\begin{aligned} m_1^{(l)} &= 1 + \sigma_w^2 d_1^{(l)}, \\ m_2^{(l)} &= 1 + \sigma_w^2 \left( 4d_1^{(l)} + \sigma_w^2 \left( d_2^{(l)} - (d_1^{(l)})^2 s_1 \right) \right). \end{aligned} \quad (31)$$

As  $\mu_{\mathbf{J}_l \mathbf{J}_l^T} = m_1^{(l)}$  and  $\sigma_{\mathbf{J}_l \mathbf{J}_l^T}^2 = m_2^{(l)} - (m_1^{(l)})^2$ , we have the following corollary.

**Corollary 1.** Assuming that  $d_1^{(l)} \neq 0$ , the expectation  $\mu_{\mathbf{J}_l \mathbf{J}_l^T}$  and variance  $\sigma_{\mathbf{J}_l \mathbf{J}_l^T}^2$  of the limiting eigenvalue density of  $\mathbf{J}_l \mathbf{J}_l^T$  are given by,

$$\begin{aligned} \mu_{\mathbf{J}_l \mathbf{J}_l^T} &= 1 + \sigma_w^2 d_1^{(l)}, \\ \sigma_{\mathbf{J}_l \mathbf{J}_l^T}^2 &= \sigma_w^2 \left( 2d_1^{(l)} + \sigma_w^2 \left( d_2^{(l)} - (d_1^{(l)})^2 (1 + s_1) \right) \right), \end{aligned} \quad (32)$$

where  $s_1$  and  $d_1, d_2$  are defined in (28) and (29), respectively.

### B. Extension to the multi-layer case

We use the important property of the S-transform (12) to extend the results of single layer to multi-layer case. Since the trace operator is *cyclic-invariant*, we have

$$S_{\mathbf{J}\mathbf{J}^T} = S_{\prod_{l=1}^L (\mathbf{I} + \mathbf{W}^l \mathbf{D}^l) (\mathbf{I} + \mathbf{W}^l \mathbf{D}^l)^T} = S_{\prod_{l=1}^L \mathbf{J}_l \mathbf{J}_l^T} = \prod_{l=1}^L S_{\mathbf{J}_l \mathbf{J}_l^T}. \quad (33)$$

We see that the S-transform of  $\mathbf{J}\mathbf{J}^T$  is simply given by the product of the S-transform of each residual unit  $\mathbf{J}_l \mathbf{J}_l^T$ . Built upon this observation, the expectation  $\mu_{\mathbf{J}\mathbf{J}^T}$  and variance  $\sigma_{\mathbf{J}\mathbf{J}^T}^2$  of the limiting eigenvalue density of  $\mathbf{J}\mathbf{J}^T$  are given as follows,

**Theorem 2** (Mean and Variance of the Limiting Spectrum Density). For  $\mathbf{J} = \prod_{l=1}^L (\mathbf{J}^l)$ , the mean and variance of the limiting eigenvalue density of  $\mathbf{J}\mathbf{J}^\top$  are given by

$$\mu_{\mathbf{J}\mathbf{J}^\top} = \prod_{l=1}^L \mu_{\mathbf{J}_l \mathbf{J}_l^\top}, \quad \sigma_{\mathbf{J}\mathbf{J}^\top}^2 = \left( \prod_{l=1}^L \mu_{\mathbf{J}_l \mathbf{J}_l^\top} \right)^2 \sum_{l=1}^L \frac{\sigma_{\mathbf{J}_l \mathbf{J}_l^\top}^2}{\mu_{\mathbf{J}_l \mathbf{J}_l^\top}^2}. \quad (34)$$

as  $N \rightarrow \infty$ .

We refer the readers to Proof 1 in Appendix for detailed deduction. Using Theorem 2, the expectation and variance of the limiting eigenvalue density of  $\mathbf{J}\mathbf{J}^\top$  can be directly computed with the results in Corollary 1 of the single layer case (32). To ensure the mean squared singular value of the input-output Jacobian to be of order  $O(1)$  for large  $L$ , we shall have  $\mu_{\mathbf{J}\mathbf{J}^\top} = O(1)$ . This order requirement further indicates that, for both Gaussian and orthogonal weights, we shall have

$$\prod_{l=1}^L (1 + d_1^{(l)} \sigma_w^2) = O(1), \quad (35)$$

using Corollary 1.

Since that setting  $d_1^{(l)} \rightarrow 0$ , or equivalently  $\phi'(z) \rightarrow 0$ , implies that almost *all* neurons are inactivated and will lead to a total failure of training, it is *necessary* to scale the weight variance with the layer number,

$$\sigma_w^2 = O\left(\frac{1}{L}\right), \quad (36)$$

to ensure that  $\mu_{\mathbf{J}\mathbf{J}^\top} = O(1)$  for large  $L$ .

For the vanilla fully connected network, the variance  $\sigma_{\mathbf{J}\mathbf{J}^\top}^2$  may still grow in an unbounded way with the layer number  $L$  even if  $\mu_{\mathbf{J}\mathbf{J}^\top} = O(1)$  [6], [11]. Only orthogonal initialization can yield a stable Jacobian spectral distribution for any choice of nonlinearity with  $\phi'(0) = 1$ . However, for deep ResNets, one can easily observe that the variance of the squared singular values of the input-output Jacobian is of order  $O(1)$  if  $\sigma_w^2 = O(1/L)$ . Therefore, we have the following corollary.

**Corollary 2.** For the ResNet which is defined as (1), it is necessary to take  $\sigma_w^2 = O(1/L)$  to ensure that  $\mu_{\mathbf{J}\mathbf{J}^\top} = O(1)$  and  $\sigma_{\mathbf{J}\mathbf{J}^\top}^2 = O(1)$ , as  $L \rightarrow \infty$ .

This observation illustrates a *universality* in the Jacobian spectrum of the deep ResNet. In particular, for both scaled Gaussian and orthogonal weights, it is necessary to take  $\sigma_w^2 = O(1/L)$  to ensure that not only the expectation but also the variance of the squared singular values of the Jacobian matrix to be of order  $O(1)$  with *any* nonlinearity, that meets the assumption made in II-A.

### C. Full spectrum characterization

We have proved that setting  $\sigma_w^2 = O(1/L)$  is necessary to keep the order of the expectation and variance of the Jacobian spectrum of ResNet, in the large  $L$  limit. We discuss the full characterization of the input-output Jacobian spectrum in this subsection. Fortunately, letting  $\sigma_w^2 = O(1/L)$  makes the deduction of the spectral density distribution of  $\mathbf{J}\mathbf{J}^\top$  tractable. Assuming that  $\sigma_w^2 = c/L$ , where  $c$  is a positive constant of order one. Then it is easy to obtain that as  $L \rightarrow \infty$ ,

$$R_{\widetilde{\mathbf{D}^l \mathbf{W}^l}}(z) = \sum_{k=1}^{\infty} r_{2k-1} z^k = \frac{cd_1^l}{L} z + O\left(\frac{1}{L^2}\right). \quad (37)$$

which leads to

$$R_{\widetilde{\mathbf{J}}_l} = R_{\widetilde{\mathbf{U} + \mathbf{D}^l \mathbf{W}^l}}(z) = 1 + \frac{cd_1^l}{L} z + O\left(\frac{1}{L^2}\right). \quad (38)$$

Here,  $r_1 = \frac{cd_1^l}{L}$  donates the mean squared radius of  $\mathbf{D}^l \mathbf{W}^l$ .

Solving  $S_{\widetilde{\mathbf{J}}_l}$  with (13) and substituting  $S_{\widetilde{\mathbf{J}}_l}$  to (18), we have,

$$S_{\mathbf{J}_l \mathbf{J}_l^\top} = 1 - \frac{cd_1^{(l)}}{L} (2z + 1) + O\left(\frac{1}{L^2}\right). \quad (39)$$

Taking the logarithm of (33) yields,

$$\begin{aligned} \ln S_{\mathbf{J}\mathbf{J}^\top}(z) &= \sum_{l=1}^L \ln \left( 1 - \frac{cd_1^{(l)}}{L} (2z + 1) \right) + O\left(\frac{1}{L^2}\right) \\ &\approx -\frac{c}{L} \sum_{l=1}^L d_1^{(l)} (2z + 1) \\ &= -\theta(2z + 1), \end{aligned} \quad (40)$$

where  $\theta \equiv \frac{c}{L} \sum_{l=1}^L d_1^{(l)}$ . Then, we obtain the S-transform of  $\mathbf{J}\mathbf{J}^T$ ,

$$S_{\mathbf{J}\mathbf{J}^T}(z) = e^{-\theta(2z+1)}. \quad (41)$$

According to (9), we have,

$$S_{\mathbf{J}\mathbf{J}^T}(z) = \frac{1+z}{zM_{\mathbf{J}\mathbf{J}^T}^{-1}(z)}. \quad (42)$$

Substituting  $z \rightarrow M_{\mathbf{J}\mathbf{J}^T}(z)$  yields,

$$S_{\mathbf{J}\mathbf{J}^T}(M_{\mathbf{J}\mathbf{J}^T}(z)) = \frac{1+M_{\mathbf{J}\mathbf{J}^T}(z)}{zM_{\mathbf{J}\mathbf{J}^T}(z)}. \quad (43)$$

According to (8),  $M_{\mathbf{J}\mathbf{J}^T}(z) = zG_{\mathbf{J}\mathbf{J}^T}(z) - 1$ . Thus,

$$S_{\mathbf{J}\mathbf{J}^T}(zG_{\mathbf{J}\mathbf{J}^T}(z) - 1) = \frac{G_{\mathbf{J}\mathbf{J}^T}(z)}{zG_{\mathbf{J}\mathbf{J}^T}(z) - 1}. \quad (44)$$

Substituting (41) to (44), we finally get the equation of the Stieltjes transform  $G_{\mathbf{J}\mathbf{J}^T}(z)$  as the following corollary.

**Corollary 3.** Taking  $\sigma_w^2 = c/L$ , where  $c$  is a positive constant, for both Gaussian and orthogonal weights, the Stieltjes transform  $G_{\mathbf{J}\mathbf{J}^T}(z)$  satisfies,

$$G_{\mathbf{J}\mathbf{J}^T}(z)e^{\theta(2zG_{\mathbf{J}\mathbf{J}^T}(z)-1)} = zG_{\mathbf{J}\mathbf{J}^T}(z) - 1, \quad (45)$$

where we define  $\theta \equiv \frac{c}{L} \sum_{l=1}^L d_1^{(l)}$ .

A recent work [14] also obtains the similar result as in Corollary 3. Different from our general case, their work makes the explicit assumption that  $\sigma_w^2 = O(1/L)$ .

Next, the detailed but brief deduction of the condition number of  $\mathbf{J}$  is provided here. The condition number is defined as the ratio of the maximal and minimal singular values of  $\mathbf{J}$ . It measures the stability of the spectrum. For the deduction of the condition number  $cond(\mathbf{J})$  of  $\mathbf{J}$ , we use a trick [21] by multiplying  $z$  on the both sides of (45),

$$zG_{\mathbf{J}\mathbf{J}^T}(z)e^{\theta(2zG_{\mathbf{J}\mathbf{J}^T}(z)-1)} = z(zG_{\mathbf{J}\mathbf{J}^T}(z) - 1). \quad (46)$$

Note that  $\frac{dz}{dG} = 0$  at the endpoints of support of the spectrum [21]. By differentiating both sides of (46), we have

$$e^{\theta(2zG_{\mathbf{J}\mathbf{J}^T}(z)-1)}(2\theta zG_{\mathbf{J}\mathbf{J}^T}(z) + 1) = z \quad (47)$$

Substitute (47) to (45) and the final result gives that

$$\lambda_{\pm} = \left(1 + \theta \pm \sqrt{\theta^2 + 2\theta}\right) e^{\pm\sqrt{\theta^2 + 2\theta}}, \quad (48)$$

where  $\lambda_{\pm}$  donate the maximal and minimal eigenvalue of  $\mathbf{J}\mathbf{J}^T$  respectively. Thus, the conditional number of the input-output Jacobian matrix  $\mathbf{J}$  is,

$$cond(\mathbf{J}) = \sqrt{\frac{\lambda_+}{\lambda_-}} = \left(1 + \theta + \sqrt{\theta^2 + 2\theta}\right) e^{\sqrt{\theta^2 + 2\theta}}. \quad (49)$$

#### IV. EXPERIMENTS

In this section, we provide empirical evidence to validate the theoretical results in Section III. Experiments on fully-connected and convolutional ResNets are performed on CIFAR-10. The standard CIFAR-10 datasets augmented with random flips and crops, and random saturation, brightness, and contrast perturbations are applied. Two commonly used optimizers: SGD-Momentum and ADAM [22] are adopted. The observation that two different methods: SGD-Momentum and ADAM give very similar results, indicates the robustness of our approach. See Section C in Appendix for the results of ADAM. Ten repeated experiments are conducted for each setting and the average results are reported here.

##### A. Fully-connected ResNet

In this case, the input dimension is reduced to  $N = 400$  with a fully-connected layer of size  $1728 \times 400$ . We train a fully-connected ResNet<sup>2</sup> of depth  $L = 100$  and width  $N = 400$  for 200 epoches with a mini-batch size of 128. Four initialization scalings:  $\sigma_w^2 = 1, c/L$ , ( $c = 1, 0.1, 0.01$ ), are explored here.

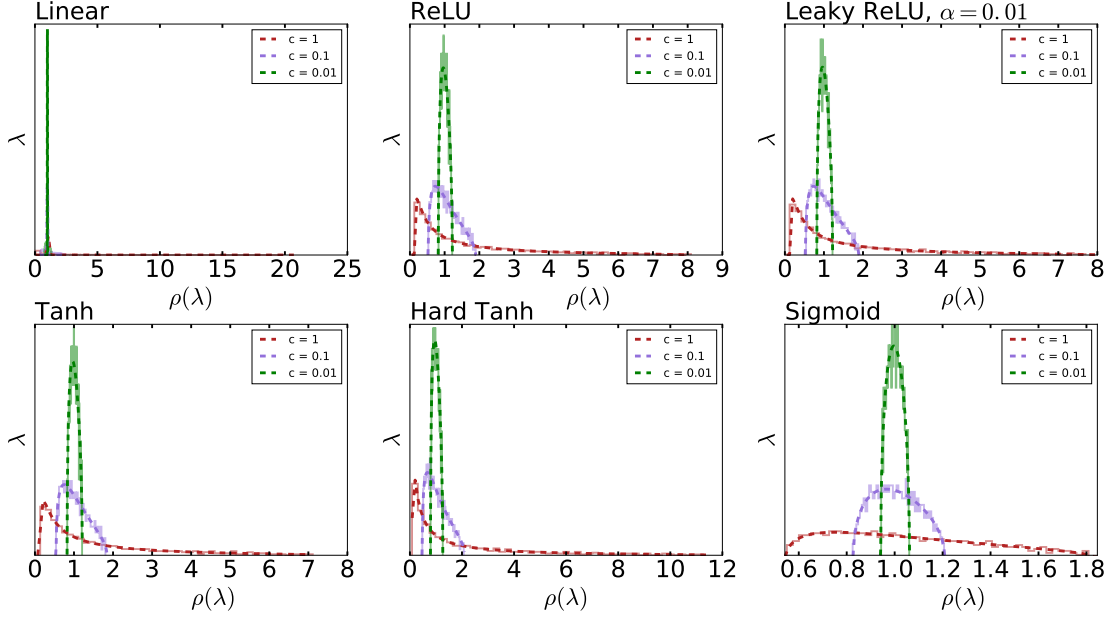


Fig. 3: Empirical eigenvalue density (solid) and limiting distribution (dashed) from  $\mathbf{J}\mathbf{J}^T$  for Gaussian weights with different  $\phi(x)$  and  $\sigma_w^2 = c/L$ ,  $N = 400$ ,  $L = 100$ .

1) *Jacobian spectrum at initialization:* In Fig. 3, we plot the empirical eigenvalue density (solid) and limiting distribution (dashed) of  $\mathbf{J}\mathbf{J}^T$  for Gaussian weights at initialization with  $\sigma_w^2 = c/L$ . Following activation functions: Linear, ReLU, Leaky ReLU, Tanh, Hard Tanh, and Sigmoid, are explored. The limiting distribution are calculated numerically with (45) and (5). Note that  $\mathbf{J}$  donates the Jacobian matrix of the output of the last residual unit in regard to the input of first one.

As shown in Fig. 3, the empirical results agree remarkably with the theoretical ones. In the cases of  $c = 1$ , different activation functions have diverse spectral density distributions because the Jacobian depends on the signal propagation. Moreover, the smaller  $c$ , the more concentrated spectrum. In the cases of the least  $c = 0.01$  (green), the spectral density distributions concentrate around one and their differences become trivial.

2) *The training performance:* In Fig. 4, we plot the training dynamics of fully-connected ResNets for the four initialization scalings with an optimal learning rate of  $10^{-3}$  and a momentum = 0.9. The training losses of  $\sigma_w^2 = 1$  are too huge to be included in Fig. 4.

As shown in Fig. 4, the magnitude of  $\sigma_w^2$  has a major influence on the learning speed. Based on our theory, an advantage of using layer-dependent scalings of  $\sigma_w^2 = c/L$  is claimed over the classical layer-independent scaling  $\sigma_w^2 = 1$ . This claim is confirmed in Fig. 4 in which the performances of  $\sigma_w^2 = c/L$  is much better than those of  $\sigma_w^2 = 1$  (blue). For the fixed nonlinearity, the smaller  $c$ , or equivalently, the more concentrated spectrum becomes at initialization, resulting in the faster learning speed. The optimal training speed is obtained with the least  $c = 0.01$  (green), which is the most isometric case. This observation indicates that the stability of the input-output Jacobian spectrum at initialization strongly predicts the training performance, especially at the early stage of training. However, the training speeds vary among experiments with different activation functions even if the Jacobian spectrum at initialization are almost the same in the cases of  $c = 0.01$  (see the green line in Fig 3). This observation indicates that the Jacobian spectrum at the initialization is not sufficient to determine the learning performance without consideration of nonlinearities. Similar results of random scaled orthogonal weights are observed in Section B in Appendix.

3) *The generalization performance:* We plot the generalization dynamics in Fig. 5. Similar with the training dynamics, the generalization performance of  $\sigma_w^2 = c/L$  is much better than  $\sigma_w^2 = 1$ . For Linear, ReLU and Leaky ReLU, the learning even failures due to the ill-conditioned Jacobian spectrum at the initialization. Moreover, the most concentrated Jacobian spectrum at initialization ( $c = 0.01$ ) is not always the best choice for generalization performance throughout training. This result indicates that the relationship between generalization and the Jacobian spectrum goes beyond simply the initialization.

<sup>2</sup> In fully-connected ResNet case, every residual unit contains a single layer without batch normalization.

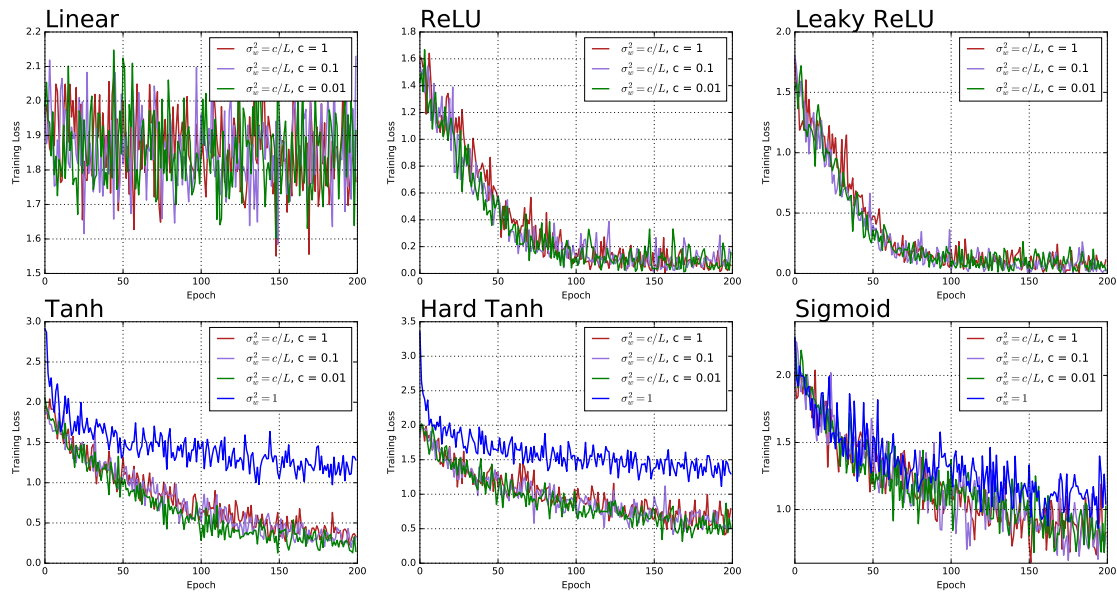


Fig. 4: Training dynamics of fully-connected ResNets for different initialization scalings of six common used activation functions with a learning rate of  $10^{-3}$  and momentum = 0.9.

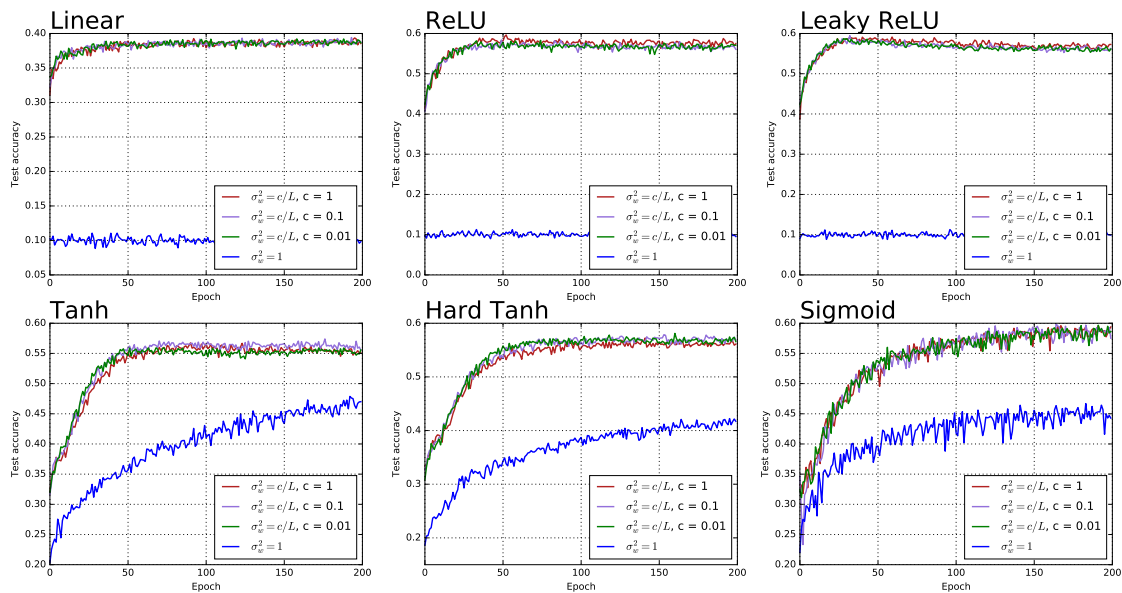
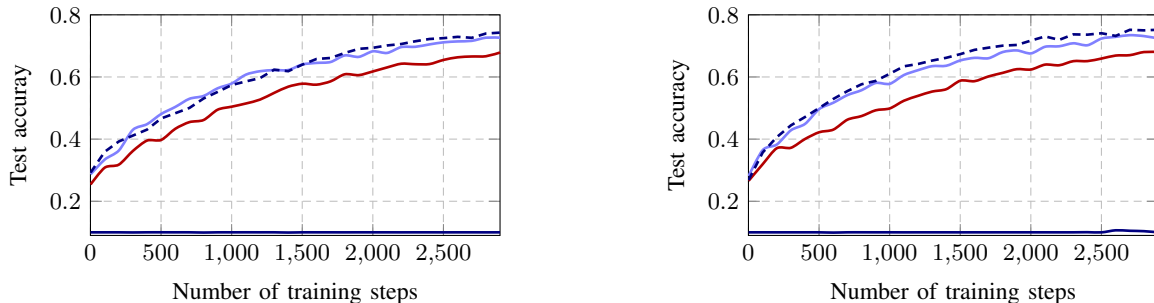


Fig. 5: The evolutions of test accuracies of fully-connected ResNets for different initialization scalings of six common used activation functions with a learning rate of  $10^{-3}$  and momentum = 0.9.

## B. Convolutional ResNet

We conduct the experiment based on the convolutional ResNet-110 structure as in [9]. In fact, we can adopt the entire analysis above into the convolutional setting with essentially no modification [23]. In this convolutional ResNet, each residual unit contains a shallow network of 2 layers. Therefore, by considering the Jacobian of *all* residual units three scalings of  $\sigma_w^2 = 1, 1/\sqrt{L}$  and  $0.01/\sqrt{L}$  are tested. In this experiment, we focus on the learning speed at the early stage of training. For the three choices of  $\sigma_w^2$ , the best performance is always achieved by the learning rate of  $10^{-2}$  with momentum = 0.9 and is presented in Fig. 6. We refer the reader to Section D in Appendix for the results of the ADAM optimizer. We observe from Fig. 6 that: 1) for convolutional ResNet without BN, the magnitude of  $\sigma_w^2$  plays a central role in obtaining a satisfying learning speed. The optimal learning speed is achieved with  $\sigma^2 = 1/\sqrt{L}$ , while large  $\sigma^2 = 1$  without BN results in exploding gradient and hence the failure of training. Surprisingly, small  $\sigma^2 = 1/\sqrt{L}$  without the regularization effect of the BN [10] *still* has roughly the same performance as  $\sigma^2 = 1$  with BN. 2) it is noteworthy that, different from the fully-connected ResNet case, for the convolutional ResNet of 2 layers in each residual unit, the scaling  $\sigma^2 = 1/\sqrt{L}$  always outperforms  $\sigma^2 = 0.01/\sqrt{L}$  while the latter achieves the *dynamical isometry*. This observation is not trivial and comes possibly from the fact that extremely small  $\sigma_w^2$  causes the internal gradient vanishing inside each residual unit. We will discuss this point in the next section.



(a) Gaussian weights with  $\mathbf{W}_{ij}^l \sim \mathcal{N}(0, \sigma_w^2/N)$

(b) Orthogonal weights with  $\mathbf{W}^l(\mathbf{W}^l)^T = \sigma_w^2 \mathbf{I}_N$

Fig. 6: Learning dynamics of a convolutional ResNet for different initialization scalings  $\sigma_w^2 = 0.01/\sqrt{L}$  (red),  $\sigma_w^2 = 1/\sqrt{L}$  (purple) and  $\sigma_w^2 = 1$  (dark blue), with a learning rate of  $10^{-2}$  and the ReLU nonlinearity. Solid lines without BN and dashed ones with the BN procedure added (for  $\sigma_w^2 = 1$ ).

## V. DISCUSSION AND CONCLUSION

In this article, exploiting advanced tools in free probability in the regime of a large network, we establish, that for ResNets, the variance of the initial random weights should *also* be scaled as a function of the number of layers. In particular, the theoretical results show that for large  $L$  the condition for spectrum concentration is in fact *universal* in the sense that, for almost *all* of the common-used nonlinearities and both weight initialization methods (Gaussian or orthogonal), it is sufficient and necessary to take  $\sigma_w^2 = O(1/L)$  to ensure the squared singular values of the input-output Jacobian to be of order  $O(1)$  (thus is neither vanishing nor exploding). The weights scaling essentially results in the *eigenspectrum concentration* of  $\mathbf{J}\mathbf{J}^T$ , such that the error vector will be properly preserved under backpropagation. We then provide in Section IV the comparison of empirical evidences with our theoretical results. Mathematically speaking, our approach holds only asymptotically as  $N, L \rightarrow \infty$ , practical advantages are observed for finite width  $N$  and depth  $L$ , when applied to the popular CIFAR-10 dataset, for both fully-connected and convolutional ResNets. This agreement is not surprising, as observed in many other fields [24]–[26].

In practice, a residual unit always contains a shallow network with  $m$  layers. In this way, the dynamic of the ResNet is given by

$$\begin{cases} \mathbf{h}_1^l &= \mathbf{W}_1^l \mathbf{x}^{l-1} + \mathbf{b}_1^l, \\ \mathbf{h}_2^l &= \mathbf{W}_2^l \phi(\mathbf{h}_1^l) + \mathbf{b}_2^l, \\ &\dots \\ \mathbf{h}_m^l &= \mathbf{W}_m^l \phi(\mathbf{h}_{m-1}^l) + \mathbf{b}_m^l, \\ \mathbf{x}^l &= \mathbf{x}^{l-1} + \phi(\mathbf{h}_m^l). \end{cases} \quad (50)$$

The entire input-output Jacobian matrix is  $\mathbf{J} = \prod_{l=1}^L (\mathbf{I}_N + \hat{\mathbf{J}}_l)$ , where  $\hat{\mathbf{J}}_l = \frac{\partial \phi(\mathbf{h}_m^l)}{\partial \mathbf{x}^{l-1}} = \prod_{i=1}^m \mathbf{D}_i^l \mathbf{W}_i^l$  denotes the local Jacobian matrix of a residual unit. For  $m > 1$ , let  $\sigma^2 = O(L^{-1/m})$  and the spectrum of  $\mathbf{J}\mathbf{J}^T$  will be well-conditioned. However, the eigenvalues of the local Jacobian matrix  $\hat{\mathbf{J}}_l \hat{\mathbf{J}}_l^T$  will be extremely small and cause the gradient vanishing in the local residual unit. Thus, a *trade-off* between the entire and local input-output Jacobian matrix is always required.

In future work, it would be interesting to extend our theoretical framework to more general skip connections. Moreover, exploring new weight initializations or nonlinearities to handle the *trade-off* mentioned above would be of practical significance.

## REFERENCES

- [1] A. Krizhevsky, I. Sutskever, and G. E. Hinton, "Imagenet classification with deep convolutional neural networks," in *Advances in neural information processing systems*, 2012, pp. 1097–1105.
- [2] A.-r. Mohamed, G. E. Dahl, and G. Hinton, "Acoustic modeling using deep belief networks," *IEEE Transactions on Audio, Speech, and Language Processing*, vol. 20, no. 1, pp. 14–22, 2012.
- [3] R. Collobert and J. Weston, "A unified architecture for natural language processing: Deep neural networks with multitask learning," in *Proceedings of the 25th international conference on Machine learning*. ACM, 2008, pp. 160–167.
- [4] X. Glorot and Y. Bengio, "Understanding the difficulty of training deep feedforward neural networks," in *Proceedings of the thirteenth international conference on artificial intelligence and statistics*, 2010, pp. 249–256.
- [5] K. He, X. Zhang, S. Ren, and J. Sun, "Delving deep into rectifiers: Surpassing human-level performance on imagenet classification," *International Conference on Computer Vision*, pp. 1026–1034, 2015.
- [6] J. Pennington, S. Schoenholz, and S. Ganguli, "Resurrecting the sigmoid in deep learning through dynamical isometry: theory and practice," in *Advances in Neural Information Processing Systems 30*, 2017, pp. 4785–4795.
- [7] A. M. Saxe, J. L. McClelland, and S. Ganguli, "Exact solutions to the nonlinear dynamics of learning in deep linear neural networks," *Computer Science*, 2013.
- [8] K. He, X. Zhang, S. Ren, and J. Sun, "Deep residual learning for image recognition," in *Computer Vision and Pattern Recognition*, 2016, pp. 770–778.
- [9] —, "Identity mappings in deep residual networks," *European Conference on Computer Vision*, pp. 630–645, 2016.
- [10] S. Ioffe and C. Szegedy, "Batch normalization: Accelerating deep network training by reducing internal covariate shift," in *Proceedings of the 32nd international conference on Machine learning*, 2015, pp. 448–456.
- [11] J. Pennington, S. S. Schoenholz, and S. Ganguli, "The emergence of spectral universality in deep networks," *International Conference on Artificial Intelligence and Statistics*, pp. 1924–1932, 2018.
- [12] M. Hardt and T. Ma, "Identity matters in deep learning," *International Conference on Learning Representations*, 2017.
- [13] G. Yang and S. Schoenholz, "Mean field residual networks: On the edge of chaos," in *Advances in Neural Information Processing Systems 30*, 2017, pp. 7103–7114.
- [14] W. Tarnowski, P. Warchol, S. Jastrzebski, J. Tabor, and M. A. Nowak, "Dynamical isometry is achieved in residual networks in a universal way for any activation function," *arXiv:1809.08848*.
- [15] A. Krizhevsky, "Learning multiple layers of features from tiny images," 2009.
- [16] S. S. Schoenholz, J. Gilmer, S. Ganguli, and J. Sohl-dickstein, "Deep information propagation," *International Conference on Learning Representations*, 2017.
- [17] A. Nica and R. Speicher, "Lectures on the combinatorics of free probability," *Cambridge Uk*, 2006.
- [18] T. Tao, *Topics in Random Matrix Theory*. American Mathematical Society, 2012.
- [19] B. Cakmak, "Non-hermitian random matrix theory for mimo channels," *Institutt for Elektronikk Og Telekommunikasjon*, 2012.
- [20] V.A.Marchenko and L.A.Pastur, "Distribution of eigenvalues for some sets of random matrices," *Mathematics of the Ussr-Sbornik*, vol. 1, no. 1, p. 507 & ndash;536, 1967.
- [21] G. Akemann, J. R. Ipsen, and M. Kieburg, "Products of rectangular random matrices: singular values and progressive scattering," *Phys Rev E Stat Nonlin Soft Matter Phys*, vol. 88, no. 5, p. 052118, 2013.
- [22] D. P. Kingma and J. Ba, "Adam: A method for stochastic optimization," *Computer Science*, 2014.
- [23] L. Xiao, Y. Bahri, J. Sohl-dickstein, S. S. Schoenholz, and J. Pennington, "Dynamical isometry and a mean field theory of cnns: How to train 10,000-layer vanilla convolutional neural networks," in *Proceedings of the 35th international conference on Machine learning*, 2018, pp. 5389–5398.
- [24] J. W. Silverstein, *Spectral analysis of large dimensional random matrices*. Science Press, 2010.
- [25] V. Plerou, P. Gopikrishnan, B. Rosenow, L. A. N. Amaral, and H. E. Stanley, "Universal and nonuniversal properties of cross correlations in financial time series," *Physical Review Letters*, vol. 83, no. 7, pp. 1471–1474, 1999.
- [26] Z. Liao and R. Couillet, "On the spectrum of random features maps of high dimensional data," *International Conference on Machine Learning*, pp. 3063–3071, 2018.
- [27] G. Ferraro, *Lagrange inversion theorem*. Springer New York, 2008.

## APPENDIX

## A. Proof of Theorem. III-B

**Proof 1** (Multi-layer case). Since

$$M_{\mathbf{J}_l \mathbf{J}_l^T} = \frac{m_1^{(l)}}{z} + \frac{m_2^{(l)}}{z^2} + \dots \quad (51)$$

Employ the Lagrange inversion theorem [27] and we have,

$$M_{\mathbf{J}_l \mathbf{J}_l^T}^{-1} = \frac{m_1^{(l)}}{z} + \frac{m_2^{(l)}}{m_1^{(l)}} + \dots \quad (52)$$

According to (33),

$$S_{\mathbf{J}_l \mathbf{J}_l^T} = \frac{1+z}{z M_{\mathbf{J}_l \mathbf{J}_l^T}^{-1}} = \frac{1}{m_1^{(l)}} + \left( \frac{1}{m_1^{(l)}} - \frac{m_2^{(l)}}{(m_1^{(l)})^3} \right) z + \dots, \quad (53)$$

Thus,

$$\begin{aligned} S_{\mathbf{J} \mathbf{J}^T} &= \prod_{l=1}^L S_{\mathbf{J}_l \mathbf{J}_l^T} \\ &= \prod_{l=1}^L \frac{1}{m_1^{(l)}} + \sum_{j=1}^L \left[ \left( \frac{(m_1^{(j)})^2 - m_2^{(j)}}{(m_1^{(j)})^2} \right) \prod_{l=1}^L \frac{1}{m_1^{(l)}} \right] z + \dots \end{aligned} \quad (54)$$

For the sake of simplicity, let  $X \equiv \prod_{l=1}^L \frac{1}{m_1^{(l)}}$  and  $Y \equiv \sum_{j=1}^L \left[ \left( \frac{(m_1^{(j)})^2 - m_2^{(j)}}{(m_1^{(j)})^2} \right) \prod_{l=1}^L \frac{1}{m_1^{(l)}} \right]$ . Expand  $M_{\mathbf{J} \mathbf{J}^T}^{-1}$  and we have,

$$M_{\mathbf{J} \mathbf{J}^T}^{-1} = \frac{1+z}{z S_{\mathbf{J} \mathbf{J}^T}} = \frac{1}{Xz} + \frac{X-Y}{X^2} + \dots \quad (55)$$

Let  $m^k := \int d\lambda \rho_{\mathbf{J} \mathbf{J}^T}(\lambda) \lambda^k$ , we obtain the following equations:

$$m_1 = \frac{1}{X} = \prod_{l=1}^L m_1^{(l)}, \quad m_2 = \frac{X-Y}{X^3}. \quad (56)$$

Finally, we obtain the expectation  $\mu_{\mathbf{J} \mathbf{J}^T}$  and variance  $\sigma_{\mathbf{J} \mathbf{J}^T}^2$  of  $\mathbf{J} \mathbf{J}^T$ ,

$$\begin{aligned} \mu_{\mathbf{J} \mathbf{J}^T} &= m_1 = \prod_{l=1}^L m_1^{(l)}, \\ \sigma_{\mathbf{J} \mathbf{J}^T}^2 &= m_2 - m_1^2 = \left( \prod_{l=1}^L m_1^{(l)} \right)^2 \sum_{l=1}^L \frac{m_2^{(l)} - (m_1^{(l)})^2}{(m_1^{(l)})^2}. \end{aligned} \quad (57)$$

## B. Fully-connected ResNets: SGD-Momentum with Random Scaled Orthogonal Weights

In Fig. 7, we plot the training dynamics of fully-connected ResNets for the four initialization scalings of scaled random orthogonal weights with six common used activation functions. The optimizer is SGD-Momentum with an optimal learning rate of  $10^{-3}$  and a momentum = 0.9. In Fig. 8, we plot the evolutions of test accuracies.

## C. Fully-connected ResNets: ADAM

1) *Random Scaled Gaussian Weights*: In Fig. 9, we plot the training dynamics of fully-connected ResNets for the four initialization scalings of scaled random Gaussian weights with six common used activation functions. The optimizer is ADAM with an initial learning rate of  $10^{-4}$ . In Fig. 10, we plot the evolutions of test accuracies.

2) *Random Scaled Orthogonal Weights*: In Fig. 11, we plot the training dynamics of fully-connected ResNets for the four initialization scalings of scaled random orthogonal weights with six common used activation functions. The optimizer is ADAM with an initial learning rate of  $10^{-4}$ . In Fig. 12, we plot the evolutions of test accuracies.

## D. Convolutional ResNet

We plot the learning dynamics of the convolutional ResNet-110 for different initialization scalings of random weight with the ReLU nonlinearity in Fig.13. The optimizer is ADAM with an initial learning rate of  $10^{-2}$ .

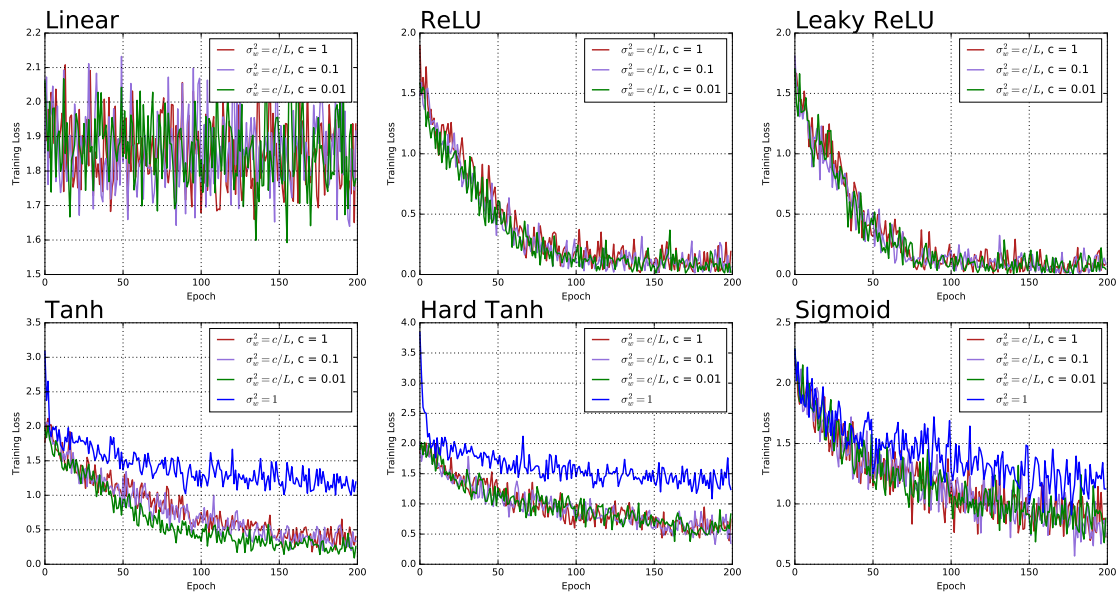


Fig. 7: Training dynamics of fully-connected ResNets for the different initialization scalings of scaled random orthogonal weights. Six common used activation functions are tested. The optimizer is SGD-Momentum with an learning rate of  $10^{-3}$  and a momentum = 0.9.

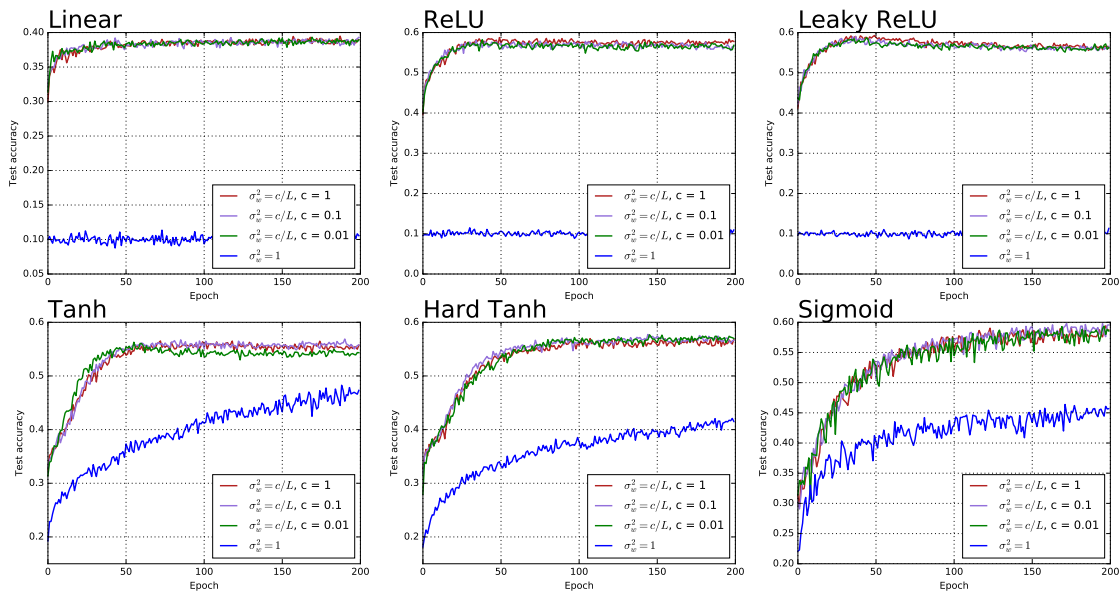


Fig. 8: The evolutions of test accuracies of fully-connected ResNets for the different initialization scalings of scaled random orthogonal weights. Six common used activation functions are tested. The optimizer is SGD-Momentum with an learning rate of  $10^{-3}$  and a momentum = 0.9.

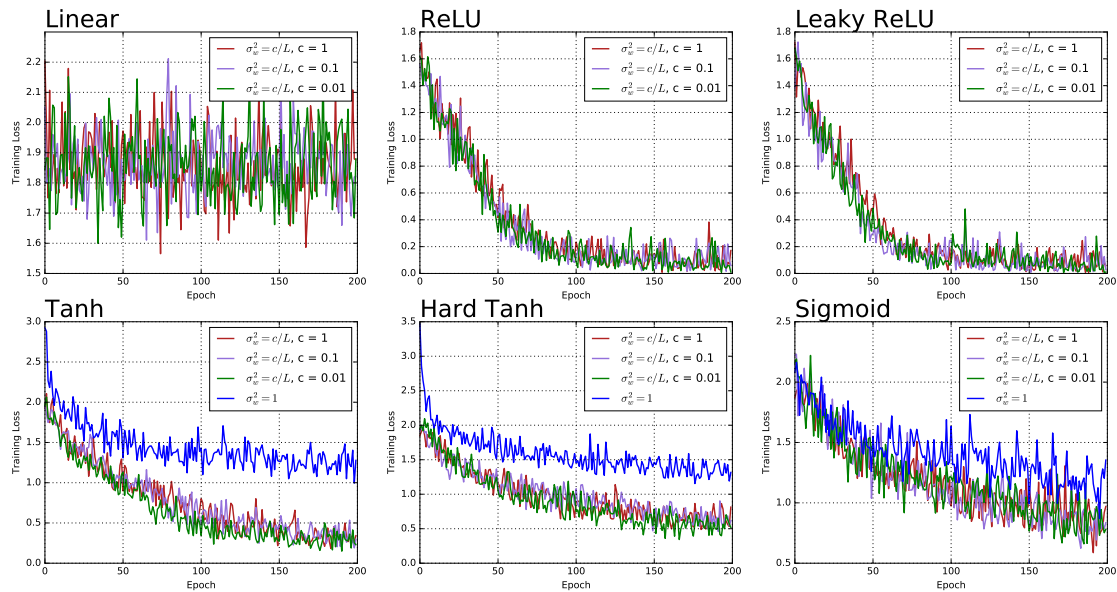


Fig. 9: Training dynamics of fully-connected ResNets for the different initialization scalings of scaled random Gaussian weights. Six common used activation functions are tested. The optimizer is ADAM with an initial rate of  $10^{-4}$ .

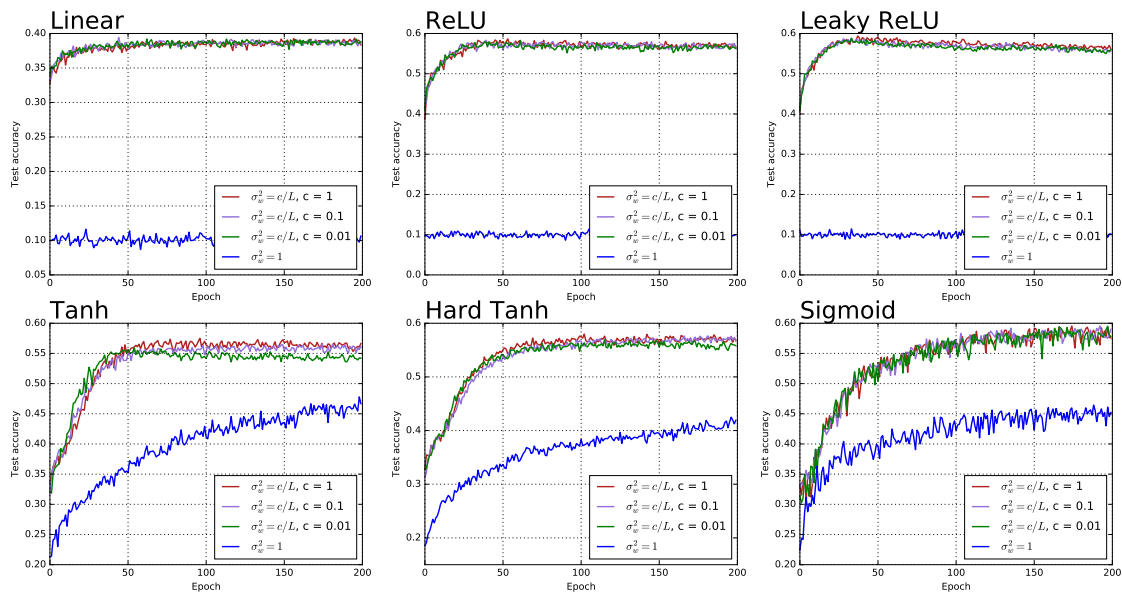


Fig. 10: The evolutions of test accuracies fully-connected ResNets for the different initialization scalings of scaled random Gaussian weights. Six common used activation functions are tested. The optimizer is ADAM with an initial rate of  $10^{-4}$ .

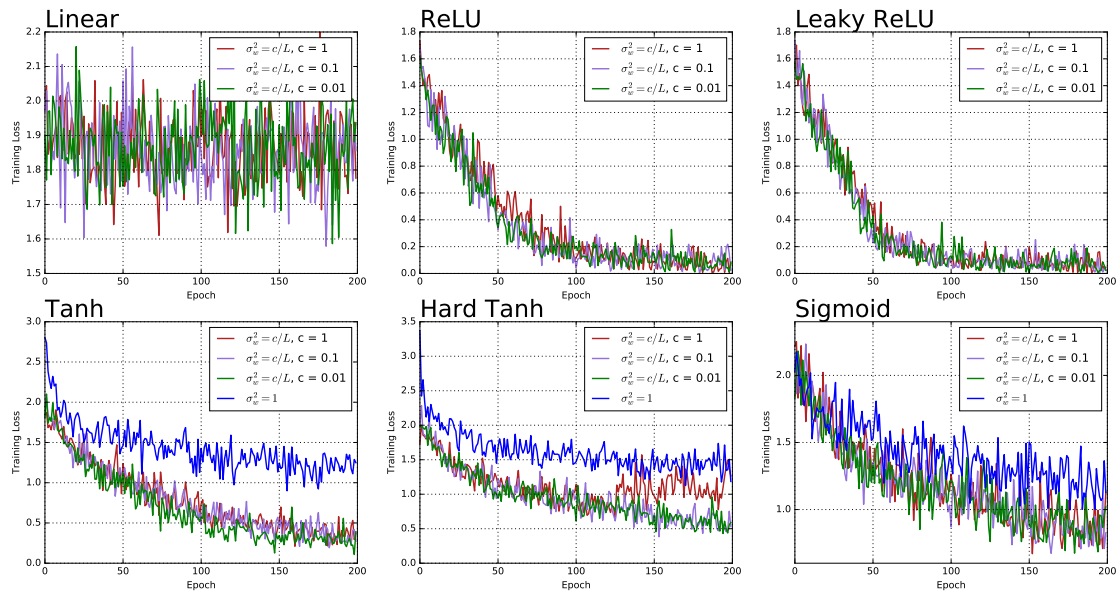


Fig. 11: Training dynamics of fully-connected ResNets for the different initialization scalings of scaled random orthogonal weights. Six common used activation functions are tested. The optimizer is ADAM with an initial rate of  $10^{-4}$ .

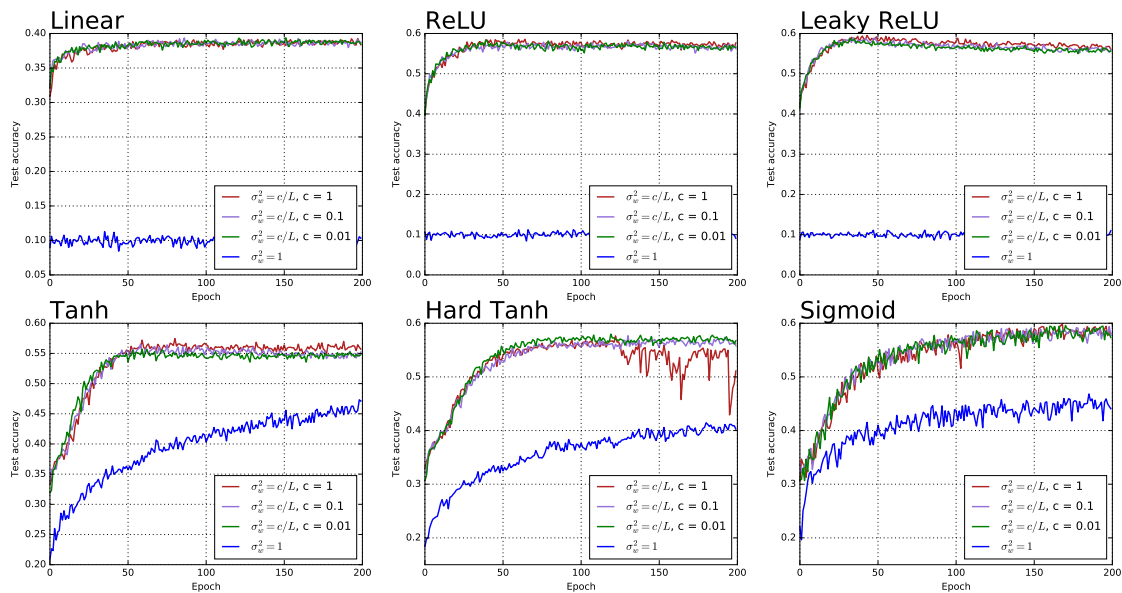


Fig. 12: The evolutions of test accuracies of fully-connected ResNets for the different initialization scalings of scaled random orthogonal weights. Six common used activation functions are tested. The optimizer is ADAM with an initial rate of  $10^{-4}$ .

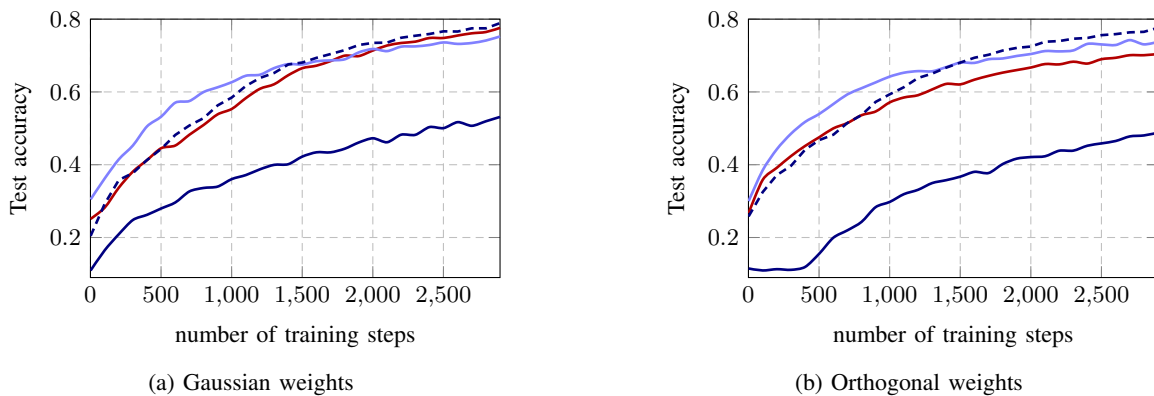


Fig. 13: Learning dynamics of a convolutional ResNet for different initialization scalings  $\sigma_w^2 = 0.01/\sqrt{L}$  (red),  $\sigma_w^2 = 1/\sqrt{L}$  (purple) and  $\sigma_w^2 = 1$  (blue), with the ReLU nonlinearity. The optimizer is ADAM with an initial learning rate of  $10^{-2}$ . Solid lines without BN and dashed ones with the BN procedure added (for  $\sigma_w^2 = 1$ ).